29. E. M. Southern, *J. Mol. Biol.* **98**, 503 (1975).
30. C. Disteche, E. Eicher, S. Latt, *Proc. Natl. Acad. Sci. U.S.A.* **76**, 5234 (1979).
31. M. Harper, A. Ullrich, G. Saunders, *ibid.* **78**, 4458 (1981).
32. M. Nesbitt and U. Francke, *Chromosoma* **41**, 145 (1973).
33. S. Tonegawa, *Nature (London)* **302**, 575 (1983).
34. P. Patten *et al.*, *ibid.* **312**, 40 (1984).
35. J. Novotny, unpublished results.
36. K. Rajewsky and K. Eichmann, in *Contemporary Topics in Immunobiology*, O. Stutman, Ed. (Plenum, New York, 1977), vol. 7, pp. 69–112.
37. M. H. Julius, A. A. Augustin, H. Cosenza, in *Regulation by T Cells*, D. G. Kilburn, J. G. Levy, T. Hung-Sia, Eds. (Univ. of British Columbia Press, Vancouver, 1979), pp. 347–371.
38. D. R. Webb, J. A. Kapp, C. W. Pierce, *Annu. Rev. Immunol.* **1**, 423 (1983).
39. S. L. Epstein, J. A. Bluestone, D. H. Sachs, in *The Biology of Idiotypes*, M. I. Greene and A. Nisonoff, Eds. (Plenum, New York, 1984), pp. 279–297.
40. Supported by NCI grants CA-28900-04 (S.T.), CA-28900-04 (H.N.E.), and CA-24051 (a core grant to S. E. Luria), by NIH grant GM 30476-03 (C.M.D.), and a postdoctoral fellowship from the Arthritis Foundation (D.M.K.)

7 December 1984; accepted 27 December 1984

Molecular Structure of Troponin C from Chicken Skeletal Muscle at 3-Angstrom Resolution

Abstract. *The x-ray structure of chicken skeletal muscle troponin C (TnC), the Ca^{2+}-binding subunit of the troponin complex, shows that the protein is about 70 angstroms long with an unusual dumbbell shape. The carboxyl and amino domains are separated by a single long α helix of about nine turns. Only the two high-affinity Ca^{2+}-Mg^{2+} sites of the COOH-domain are occupied by metal ions resulting in conformational differences between the COOH- and NH_2-domains. These differences are probably important in the triggering of muscle contraction by TnC. Also the structure of TnC is relevant in understanding the function of other calcium-regulated proteins, in particular that of calmodulin because of its strong similarity in amino acid sequence.*

Muscle contraction involves the relative sliding of interdigitating myosin- and actin-containing filaments. This process is controlled by the two actin-associated proteins troponin and tropomyosin (*1*). Troponin contains three subunits: troponin T (TnT), which binds the troponin complex to tropomyosin, troponin I (TnI), which inhibits actomyosin adenosine triphophatase activity and troponin C (TnC) which binds four Ca^{2+} ions (*2, 3*). Calcium binding to TnC causes large conformational changes in the protein, which alters protein-protein interactions in the other thin filament proteins—namely, TnI, TnT, tropomyosin, and actin—leading to the muscle contractile process.

TnC (the molecular weight is 18,000) binds four Ca^{2+} ions; two in low-affinity, Ca-specific sites and two in high-affinity sites, which can also bind Mg^{2+} (*4*). The Ca-binding sites are each thought to be flanked by a pair of helices because of amino acid sequence similarities to Ca sites in parvalbumin (*5*). Details of the three-dimensional structure are essential for understanding (i) the stereochemistry of the specificity and selectivity of the metal-ion binding domains and (ii) the relation between TnC and the contractile mechanism.

Reports on the crystallization and diffraction of chicken TnC (*6, 7*) have shown that the crystals belong to the space group $P3_221$ with unit cell dimensions of $a = b = 66.7$ Å, $c = 60.8$ Å, and $\gamma = 120°$. We now report the three-dimensional structure of chicken TnC at 3.0-Å resolution. The structure was solved with the use of a single isomorphous neodymium heavy-atom derivative at 3.8-Å resolution and the application of a novel phase improvement and phase extension procedure to 3-Å resolution (*8*). Crystals of the corresponding turkey TnC (*9*) have the same trigonal space group, and have unit cell constants similar to those of chicken TnC. A preliminary report of the structure of turkey TnC has been presented (*10*).

Troponin C was isolated from breast and leg muscles of chicken and purified (*3*). The protein was crystallized by vapor diffusion method at 8°C, and the reservoir buffer contained 50 m*M* sodium acetate, *p*H 4.9, 5.0 m*M* $MnCl_2$ and 1.0 m*M* NaN_3 in 43 percent saturated ammonium sulfate. The details for crystallization and crystallographic data have been described (*6, 7*).

Intensity data including equivalent reflections and Friedel pairs were collected on the Enraf-Nonius CAD-4 diffractometer with the θ-2θ scan mode. The data were reduced and scaled in the usual way (*11*).

Heavy atom reagents were examined for suitability in the preparation of isomorphous derivatives. Many of the resulting crystals produced large intensity changes, but the difference Patterson maps (*12*) were not interpretable. However, the lanthanides [$TbCl_3$, $Sm(NO_3)_3$, $NdCl_3$, $LaCl_3$], produced the same single site derivative but with varying occupancies of which neodymium (Nd) was the greatest. A different single site derivative for gold was also obtained with $KAu(CN)_2$. The heavy atom sites in the Nd or Au derivative were refined by means of the centrosymmetric set of *h*0*l* reflections. The space group was established as $P3_221$ (rather than $P3_121$) with the use of the anomalous data and SIRAS (single isomorphous replacement data set with anomalous scattering) phases from the Nd derivative to reproduce the known site in the gold derivative. When the two derivatives, Au at 5.0 Å and Nd at 3.8 Å resolution (*13*), were used, 1190 native reflections were phased with an overall figure of merit of 0.78. The "best" (*14*) electron density map showed secondary structural features but was not completely interpretable.

The phase improvement and phase extension were carried out with a novel iterative procedure developed by Wang (*8, 15*). At the start, the single isomorphous replacement (SIR) and the anomalous scattering (SAS) phasing statistics for Nd, La, Tb, and Au were calculated. The statistics showed (Table 1) that Tb and Au had lower phasing power. Therefore, the analysis was carried out with only Nd and La derivative data, and the four data sets (SIR and SAS for Nd at 3.8 Å and SIR and SAS for La at 4.5 Å) were merged into a single data set. Since the Nd and La derivatives had a single com-

Table 1. Some initial statistics aiding the selection of TnC derivatives.

Derivative	Resolution (Å)	SIR data		SAS data	
		*R** (Cullis)	Figure of merit	*R*† (acentric)	Figure of merit
Nd	3.8	0.547	0.40	0.323	0.42
La	4.5	0.537	0.42	0.341	0.42
Au	4.0	0.604	0.33	0.515	0.20
Tb	5.6	0.574	0.42	0.301	0.45

*R (Cullis) = $\Sigma||\Delta F_{obs}| - |F_{Hcal}||/\Sigma|\Delta F_{obs}|$, where ΔF_{obs} is the observed structure factor difference between the heavy atom derivative and the native and F_{Hcal} is the calculated heavy atom contribution. The summation is taken over only the centric reflections. †R (acentric) = $\Sigma||\Delta F''_{obs}| - |F''_{Hcal}||/\Sigma|\Delta F''_{obs}|$, where $\Delta F''_{obs}$ is the Bijvoet difference in the derivative data and F''_{Hcal} is the calculated imaginary component of the heavy atom contribution. The summation is taken over 25 percent acentric reflections with the largest $\Delta F''_{obs}$.

mon site (at $x = 0.200$, $y = 0.040$, and $z = 0.040$) the merged data set (containing 1375 reflections) was essentially SIRAS information. The phase improvement process was carried out by first identifying the protein-solvent boundary in the structure with an iterative procedure (*15*). With this information, a direct-space filter was constructed, and the process was iterated for four cycles. Then a new filter was generated and the process repeated for four more cycles starting from the original SIRAS phases. After eight cycles of phase improvement, the extension to 3.0 resolution was started, first from 3.8 Å to 3.3 Å and then from 3.3 Å to 3.0 Å with four cycles of iteration in each stage. At the end of the process, a total of 2782 reflections were phased, which is nearly double the number of 1375 starting phases at 3.8 Å. Thus phases were generated for 1407 reflections (between 3.8 Å and 3.0 Å) that had no previous phase information.

An anomalous Fourier map calculated with these phases for both Nd and La data sets showed a minor site (at −0.131, 0.090, 0.072) at a height of 25 percent of the lanthanide site. This site did not appear in the difference maps when the Nd or La data and the native data were used. Inclusion of this additional minor site lowered the acentric R (Table 1) from 0.323 to 0.300 for Nd and 0.341 to 0.307 for La. This minor site was included and the entire procedure was again repeated. The final figure of merit for all the 2782 reflections at 3.0-Å resolution was 0.84. The average change in phase for the 1375 reflections with SIRAS phases at 3.8-Å resolution was 20° and for the entire set of 2782 reflections at 3.0 Å was 56° (*16*). Some representative electron density maps showing the results before and after this phase improvement and extension process are given in Fig. 1.

The 3.0-Å resolution electron density map was sectioned along the z axis at intervals of 0.9 Å, and the sections were stacked and studied. The most striking feature of the map, which revealed the molecular boundary, was the extremely well-defined long helical stem consisting of about nine turns and connecting the globular NH_2- and COOH-terminal domains. The backbone chain trace began with the long central helix and progressed toward both domains. The helix-loop-helix alternation in the secondary structure aided in the interpretation of the electron density map. All the helices were right-handed and, except for the

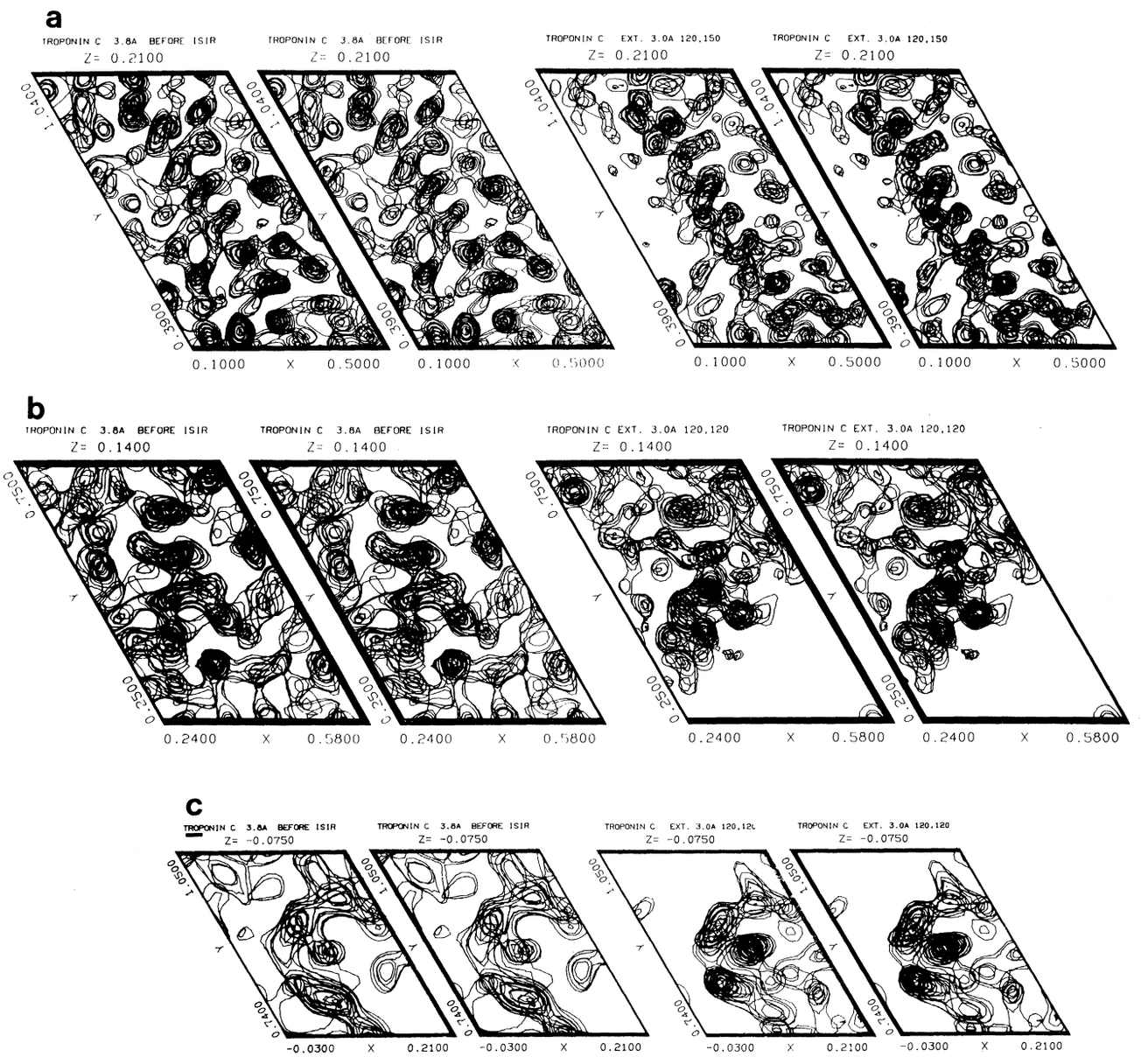

Fig. 1. Representative stereo pairs of the extent of map improvement before (left) and after (right) the phase improvement and phase extension process. (a) Electron density sections in the region of the long continuous helix. (b) Electron density sections of the NH_2-terminal (NT) helix. (c) Electron density of a segment of the Ca^{2+}-binding loop (site IV).

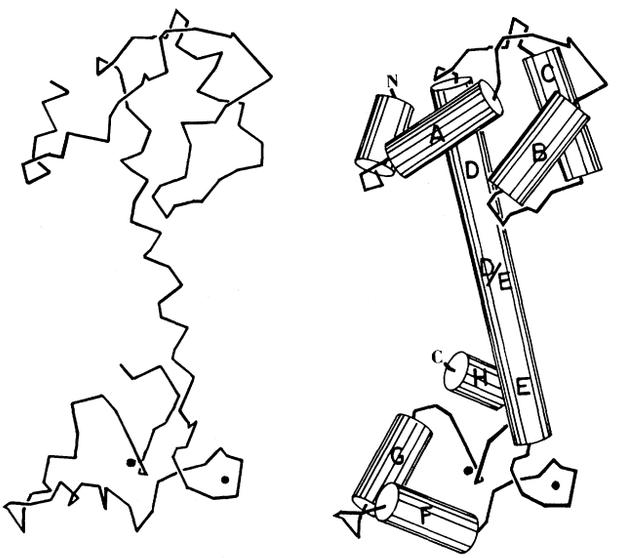

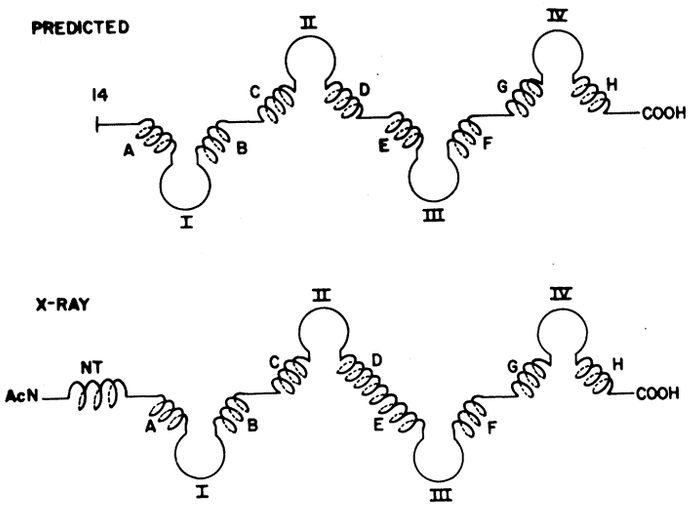

Fig. 2 (left). A model of the backbone trace of chicken TnC (left) and a drawing of the structure (right). Closed circles represent the two metal sites. Fig. 3 (right). The predicted and observed secondary structure of chicken TnC.

long central helix, consisted of about three turns. Both of the expected Ca^{2+}-Mg^{2+} sites (III and IV) in the COOH-domain are occupied in the native structure either by Ca^{2+} or Mn^{2+} (since Mn^{2+} is present in the crystallization medium). One of these sites (site III) is occupied by Nd^{3+} in the heavy-atom derivative. The distance between these two metal sites is 11.3 Å. The backbone and many of the side chains were clear. A model of the backbone trace and a schematic drawing of the TnC is shown in Fig. 2 (*17*).

The observed structure of TnC is most unusual in that a single long right-handed α-helix of about nine turns spans the globular NH_2- and COOH-domains. The overall length of the molecule is about 70 Å. This structure is different from the proposed model for TnC with Ca^{2+} found at all four sites (*18*); specifically, the long central helix results from the D helix, the D-E linker, and the E helix of the predicted structure (Fig. 3). The expected four helices—three short helices of about three turns each plus the end of the long central helix—are present in each domain (Fig. 2). The NH_2-domain, in addition, contains a short helix near the NH_2-terminus, and the four short helices surround the D helix, the NH_2-terminal end of the long helix.

TnC has four metal binding sites—two high-affinity Ca^{2+}-Mg^{2+} sites in the COOH-domain and two Ca^{2+}-specific low-affinity sites in the NH_2-domain. The x-ray structure shows that only the two sites in the COOH-domain are occupied by metal, but no metals were found in either of the two putative Ca^{2+}-binding sites of the NH_2-domain probably because of the low *p*H used in the crystallization. The two Ca^{2+}-binding helix-loop-helix configurations (E and F helices and G and H helices) of the COOH-domain are approximately at right angles to each other and are similar to the "EF-hand" (*19, 20*) of the Ca^{2+}-binding regions of parvalbumin and intestinal Ca^{2+}-binding protein (*19, 21, 22*).

In contrast, the two putative Ca^{2+}-binding folds in the NH_2-domain are very different from those of either the COOH-domain or other known Ca^{2+}-binding proteins parvalbumin and intestinal Ca^{2+}-binding protein. The A and B helices are antiparallel, whereas the C and D helices are somewhat skewed. This suggests that, when Ca^{2+} is not bound, the geometry of the helix-loop-helix is somewhat different from the standard EF-hand. Such differences in the conformation accompanying the binding of Ca^{2+} may provide a molecular basis for the understanding of the Ca^{2+}-induced conformational changes in TnC and of the propagation of these changes to TnI, TnT, tropomyosin, and actin leading to muscle contraction.

Thus the difference in the structures of the NH_2- and COOH-domains and their metal-binding specificities and affinities are dependent on the subtle sequence effects of the two domains. Although there is a striking homology between the NH_2- and COOH-terminal domains of TnC, the binding constants for Ca^{2+} do differ ($K_a \simeq 10^5 M^{-1}$ for the NH_2-domain and $\simeq 10^7 M^{-1}$ for the COOH-domain) (*1, 4*). This is probably due either to the relative importance of the hydrophobic interactions in the two domains with and without Ca^{2+} or, in contrast, to the presence of a Gly residue in the fourth position of the Ca^{2+}-binding loop. The occurrence of more than one Gly in the loop appears to generally lower the Ca^{2+}-binding affinity (*1*) probably arising from an enhanced conformational flexibility of the loop (*23*). The x-ray structure shows a clustering of hydrophobic residues (for example, Phe, Ile, Val) in the core of the NH_2-domain produced by the distinctive organization of the helices. Nuclear magnetic resonance studies had also shown that (in rabbit TnC) hydrophobic interactions (involving Phe^{19}, Phe^{23}, and Phe^{26} of the A helix and Phe^{72} and Phe^{75} of the D helix) stabilize the NH_2-terminal domain in the absence of Ca^{2+}, whereas the reverse is the case in the COOH-domain, where the hydrophobic interactions apparently stabilize the Ca^{2+}-bound state (*24–27*). Therefore, there must be a delicate balance between the hydrophobic interaction energy of the NH_2-domain in the metal-free state and the ionic interaction energy on Ca^{2+} binding to the loops (*27*). The conformational transition between the metal-bound and metal-free states is apparently regulated by the concentrations of Ca^{2+} in the cell cytosol, and this in turn depends on Ca^{2+} binding and release by the sarcoplasmic reticulum. After nerve stimulation, the increase in Ca^{2+} ion concentration (10^{-5} *M*) results in the uptake of Ca^{2+} by the NH_2-domain of TnC; this leads to the Ca^{2+}-induced conformational change in TnC, the key step in the initiation of muscle contraction.

The structure of TnC is not only of significance because of the role of the protein in the regulation of muscle contraction, but also because of the similarity of its amino acid sequence to that of calmodulin, a calcium-controlled regulatory protein (*28*). The main differences

are the absence of the first 12 residues at the NH_2-terminal end in calmodulin and a D-E linker shortened by three residues. The four Ca^{2+} sites in calmodulin have binding constants ($K_a \simeq 10^5 M^{-1}$) similar to the lower affinity, Ca^{2+} specific sites in the NH_2 domain of TnC (*29*). Whether calmodulin assumes a structure similar to that of TnC and undergoes similar structural perturbations upon metal binding remains to be determined.

M. SUNDARALINGAM,* R. BERGSTROM
G. STRASBURG, S. T. RAO
P. ROYCHOWDHURY
Department of Biochemistry, College of Agricultural and Life Sciences, University of Wisconsin–Madison, Madison 53706
M. GREASER
Muscle Biology Laboratory, University of Wisconsin–Madison
B. C. WANG
Biocrystallography Laboratory, Veterans Administration Medical Center, Pittsburgh, Pennsylvania 15240, and *Crystallography Department, University of Pittsburgh, Pittsburgh, Pennsylvania 15260*

References

1. P. C. Leavis and J. Gergely, *CRC Crit. Rev. Biochem.* **16**, 235 (1984).
2. M. L. Greaser and J. Gergely, *J. Biol. Chem.* **246**, 4226 (1971).
3. ———, *ibid.* **248**, 2125 (1973).
4. J. D. Potter and J. Gergely, *ibid.* **250**, 4628 (1975).
5. J. H. Collins, J. D. Potter, M. J. Horn, G. Wilshire, N. Jackman, *FEBS Lett.* **36**, 268 (1973).
6. G. M. Strasburg, M. L. Greaser, M. Sundaralingam, *J. Biol. Chem.* **255**, 3806 (1980).
7. G. M. Strasburg, M. L. Greaser, S. T. Rao, M. Sundaralingam, in *Calcium-Binding Proteins and Calcium Function*, F. L. Siegel *et al.*, Eds. (Elsevier North-Holland, New York, 1980), p. 289.
8. The method has been implemented into an integrated program package called ISIR-ISAS process, was reported at the 13th International Union of Crystallography Congress held at Hamburg, Germany, 9 to 18 August 1984. [See B. C. Wang *et al., Acta Cryst.* **40A**, C12 (1984)]. An early objective of the method was to resolve the phase ambiguity problem in a single isomorphous derivative without anomalous scattering information or in a single wavelength anomalous scattering data set. A brief description of this application is also presented in *Diffraction Methods in Biological Macromolecules* (a volume of *Methods of Enzymology*), H. Wyckoff, Ed. (Academic Press, New York, in press.)
9. O. Herzberg, K. Hayakawa, M. N. G. James, *J. Mol. Biol.* **172**, 345 (1984).
10. O. Herzberg and M. N. G. James, *Acta Cryst.* **40A**, C37 (1984). Abstract 02.1-40 of paper presented at the XIII International Union of Crystallography Congress, Hamburg, Federal Republic of Germany, 9 to 18 August (1984).
11. For example, see J. Hogle *et al.*, *Acta Cryst.* **B37**, 591 (1981).
12. The difference Patterson maps were calculated with coefficients $(|F_D| - |F_N|)^2$ where D and N refer to the derivative and native structure amplitudes, respectively.
13. The data set on Nd extended to 3 Å resolution and on Au to 4-Å resolution. However, useful phasing power extended only to 3.8 Å and 5 Å, respectively.
14. D. M. Blow and F. H. C. Crick, *Acta Cryst.* **12**, 794 (1959).
15. B. C. Wang, *ibid.*, in press. The method first transforms the original Fourier map into a new map based on the density values contained within a sphere of a certain radius around each point, which depends on the resolution of the map; in the case of TnC at 3.8-Å resolution, it was 10 Å. This new map is related to the probability of finding molecules instead of atoms. The protein solvent boundary is then located from this "probability" map and with the known solvent content of the crystal. In the case of TnC, a value of 40 percent was used. The transformation process, which involves a summation of density from the original Fourier map, invokes the concept that a molecule is an assemblage of atoms; thus for the purpose of locating molecules, the new map is more suitable than the conventional map, which is used for describing individual atoms rather than molecules. The summation process will transform the true signal but not the noise in the map because the noise generally occurs as a higher frequency component in the density. Thus, the noise can be filtered out by the summation process. Therefore, such a transformation can produce a map with an error-free signal of the molecule and can allow an accurate determination of the protein-solvent boundary even when a high level of noise is present in the original map.
16. The starting phase angles for the 1407 reflections having no previous phase information were arbitrarily set to 0°.
17. The molecules are packed with the long helix lying over the internal 3_2-axis of the unit cell. The NH_2- and COOH-domains of the 3_2-axis related molecules are tightly packed and are in close contact with each other and with other symmetry-related molecules. This tight packing made it difficult to carve out the molecular boundary in our earlier work at 3.8-Å resolution which resulted in tracing the molecular boundary incorporating the NH_2- and COOH-domains of two different molecules. After the phase improvement and extension, not only was the backbone trace clear, but also the intermolecular boundary.
18. R. H. Kretsinger and C. D. Barry, *Biochim. Biophys. Acta* **405**, 40 (1975).
19. R. H. Kretsinger and C. E. Nockolds, *J. Biol. Chem.* **248**, 3313 (1973).
20. The EF-hand describes the nearly perpendicular arrangement of the E and F helices flanking the 12-residue Ca^{2+}-binding loop, in analogy to the stretched out right hand with the forefinger (E helix) and thumb (F helix) and the remaining fingers folded to form the Ca^{2+}-binding loop. The terminology was first used to describe the Ca^{2+}-binding helix-loop-helix configuration in parvalbumin (*19*).
21. D. M. E. Szebeny, S. K. Obendorf, K. Moffat, *Nature (London)* **294**, 327 (1981).
22. It is conceivable that the NH_2-domain assumes a different helix-loop-helix configuration on Ca^{2+} binding. Circular dichroism data (*2, 3*) indicate that, while Ca^{2+} binding to the COOH-domain results in a large increase in helix content, the same is not true for the NH_2-domain. This may simply mean that the expected helices of the NH_2-domain are already preformed in the metal-free state and perhaps undergo a tertiary structural rearrangement. In contrast, the increased helix content on Ca^{2+} binding to the COOH-domain has been attributed to the formation of the E and G helices (*2, 3*). It is also possible that the D-E linker helix found in the x-ray structure is formed on Ca^{2+} binding to the COOH-domain, and contributes to the exhanced helix content of the molecule.
23. In parvalbumin and intestinal Ca^{2+}-binding protein, the Ca^{2+}-binding loops differ in glycine content. The lower K_a values ($10^5 M^{-1}$) are probably associated with the presence of more than one glycine in the Ca^{2+}-binding loops, whereas the loops with higher K_a values ($10^7 M^{-1}$) are associated with the presence of only one glycine. In calmodulin, all four loops contain two glycines and show lower K_a values for the four sites.
24. For example, see J. Gergely and P. C. Leavis, in *Muscle Contractions: Its Regulatory Mechanisms*, S. Ebashi *et al.* Eds. (Springer-Verlag, Berlin, 1980), p. 191.
25. P. C. Leavis, J. Gergely, Z. Grabarek, W. Drabikowski, B. A. Levine, in *Calcium-Binding Proteins and Calcium Function*, F. L. Siegel *et al.*, Eds. (Elsevier North-Holland, New York, 1980), p. 271.
26. Many of the biophysical observations on TnC and its fragments in solution are consistent with the x-ray structure. See also B. A. Levine, D. Mercola, D. Coffman, J. M. Thornton *J. Mol. Biol.* **115**, 743 (1977); K. B. Seamon, A. J. Hartshorne, A. A. Bothner-By, *Biochemistry* **16**, 4039 (1977).
27. The combined hydrophobic and ionic stabilization energies of the Ca^{2+}-bound COOH-domain may be expected to be higher than the essentially hydrophobic interaction energy of the metal-free state. In contrast, in the NH_2-domain, the hydrophobic interaction energy may be higher in the metal-free state than the combined hydrophobic and ionic interaction energies on Ca^{2+} binding. Better insights on the molecular properties of TnC should be available when the higher resolution structure of TnC, the apo-protein and the four-Ca^{2+} protein become available.
28. W. Y. Cheung, *Science* **207**, 19 (1980).
29. J. D. Potter *et al.*, in *Calcium-Binding Proteins and Calcium Function*, R. H. Wasserman *et al.*, Eds. (Elsevier, Amsterdam, 1977), p. 239.
30. We thank Drs. C. B. Stout, W. Furey, Jr., and J. Rose of the Department of Crystallography, University of Pittsburgh and Biocrystallography Laboratory, Veterans Administration Medical Center, Pittsburgh, for their enthusiastic help with their MMS-X graphics system. Supported by an NIH grant AM-34139 and grants from the College of Agricultural and Life Sciences and the Graduate School of the University of Wisconsin–Madison.
* To whom correspondence should be addressed.

12 December 1984; accept 25 January 1985

Effects on *Trichinella spiralis* of Host Responses to Purified Antigens

Abstract. *Purification of two antigens (48-kilodalton polypeptide and a group with major subunits of 50 and 55 kilodaltons) from the infective larvae of the parasitic nematode* Trichinella spiralis *was recently reported. Immunization of mice with either of these antigens induces strong resistance to a subsequent challenge infection. In the study reported here the mechanism of this resistance was investigated by monitoring the parasite's life cycle in mice immunized with the antigens. Immunized mice were able to expel intestinal adult worms and to inhibit the fecundity of adult female worms at an accelerated rate compared to control mice. Accelerated expulsion and inhibition of fecundity may account entirely for the level of resistance induced by immunization. Although the effects of the immune response apparently are exerted on adult worms, the target antigens are expressed only by developing larvae. This suggests that immune effector mechanisms act on intestinal larvae in such a way that they develop into defective adults.*

Infection with the parasitic nematode *Trichinella spiralis* stimulates complex, stage-specific immunologic responses in the mammalian host. These responses inhibit development of the parasite at several points in its life cycle. Ultimately, they can limit the production and perhaps the migration of the newborn